Water Research 88 (2016) 135–143

Contents lists available at ScienceDirect

Water Research

journal homepage: www.elsevier.com/locate/watres

Unveiling the photoelectrocatalytic inactivation mechanism of *Escherichia coli*: Convincing evidence from responses of parent and anti-oxidation single gene knockout mutants

Hongwei Sun [a, d], Guiying Li [a], Taicheng An [a, *], Huijun Zhao [b], Po Keung Wong [c, **]

[a] The State Key Laboratory of Organic Geochemistry and Guangdong Key Laboratory of Environmental Protection and Resources Utilization, Guangzhou Institute of Geochemistry, Chinese Academy of Sciences, Guangzhou, China
[b] Centre for Clean Environment and Energy, Griffith University, Gold Coast Campus, QLD, Australia
[c] School of Life Sciences, The Chinese University of Hong Kong, Hong Kong Special Administrative Region
[d] University of Chinese Academy of Sciences, Beijing, China

ARTICLE INFO

Article history:
Received 14 July 2015
Received in revised form
29 September 2015
Accepted 2 October 2015
Available online 14 October 2015

Keywords:
Photocatalytic disinfection
Catalase
Superoxide dismutase
Oxidative stress
Hydrogen peroxide

ABSTRACT

This study investigated photoelectrocatalytic (PEC) inactivation mechanism of bacteria using parental *Escherichia coli* (*E. coli*) BW25113 and its isogenic mutants deficient in catalase HPI (*katG*$^-$, JW3914-1) and Mn-SOD (*sodA*$^-$, JW3879-1). BW25113 in the mid-log phase was less susceptible to PEC inactivation than those in early-log and stationary phases, consistent with the peak activities of catalase and superoxide dismutase (SOD) at mid-log phase (30.6 and 13.0 Unit/ml/OD_{600}). For different strains all in mid-log phase, PEC inactivation efficiency followed the order *katG*$^-$ > *sodA*$^-$ > BW25113, with the duration of 60, 60 and 90 min for complete inactivation of ~2 × 10^7 CFU mL^{-1} bacteria, respectively. Correspondingly, catalase and SOD levels of BW25113 were also higher than the mutants by 5.9 and 11.7 Unit/mL/OD_{600}, respectively. Reactive oxygen species (ROSs) concentrations in PEC systems revealed that the inactivation performance coincided with H_2O_2 levels, rather than $^{\bullet}OH$. Moreover, pre-incubation with H_2O_2 elevated catalase activities and PEC inactivation resistance of BW25113 were positively correlated. The above results indicated that H_2O_2 was the dominant PEC generated bactericide, and anti-oxidative enzymes especially catalase contributed greatly to the bacterial PEC resistance capacity. Further tests revealed that PEC treatment raised the intracellular ROSs concentration by more than 3 times, due to the permeated H_2O_2 and its intracellular derivative, $^{\bullet}OH$. However, oxidative stress response of *E. coli*, such as increased catalase or SOD were not observed, perhaps because the ROSs overwhelmed the bacterial protective capacity. The accumulated ROSs subsequently caused oxidative damages to *E. coli* cells, including membrane damage, K^+ leakage, and protein oxidation. Compared with BW25113, the mutants experienced damages earlier and at higher levels, confirming the essential roles of catalase and SOD in the bacterial PEC resistance.

1. Introduction

Aquatic pathogens are a major cause of disease; when present, drinking water must be inactivated. Traditionally widely-used chlorinated disinfection techniques have been criticized for generating hazardous by-products (Kulkarni and Chellam, 2010). Photocatalytic (PC) technology based on semiconductors has been explored as a promising candidate for water disinfection, because of its solar-driven potential and self-cleaning capacity (Rincon and Pulgarin, 2007; Dalrymple et al., 2010; Foster et al., 2011; Wang et al., 2012; Gao et al., 2013; Shi et al., 2015). Semiconductors, like TiO_2, can absorb photon energy and generate hole (h^+) and electron (e^-) pairs, subsequently reacting with H_2O and O_2 to form reactive oxygen species (ROSs) such as $^{\bullet}OH$, $^{\bullet}O_2^-$, and H_2O_2. These ROSs can simultaneously inactivate bacteria and degrade the cellular component or metabolites (Robertson et al., 2012). Another alternative, called a photoelectrocatalytic (PEC) system, applies a potential bias using the immobilized catalyst as a photoanode, enhancing inactivation performance by suppressing h^+ and e^-

* Corresponding author.
** Corresponding author.
E-mail addresses: antc99@gig.ac.cn (T. An), pkwong@cuhk.edu.hk (P.K. Wong).

http://dx.doi.org/10.1016/j.watres.2015.10.003
0043-1354/

recombination (Baram et al., 2007; Li et al., 2011, 2015). However, PC and PEC inactivation mechanisms have not yet been well established. In particular, it is important to better understand how PC or PEC inactivation impacts bacterial responses and oxidative damages.

Important to this topic is understanding two bacterial anti-oxidative enzymes: catalase and superoxide dismutase (SOD). Catalase catalyzes H_2O_2 decomposition to H_2O and O_2, while SOD catalyzes $^{\bullet}O_2^-$ to form H_2O_2 and O_2 (Chiang and Schellhorn, 2012). Leung et al. (2008) discovered the increase of catalase and SOD activities during PC treatment of marine bacteria, indicating that the oxidative stress responses were induced by the over-production of ROSs during the PC inactivation process. However, the impact of catalase or SOD on inactivation performance is not well understood; more investigation is needed to understand the roles of catalase and SOD in the PC or PEC inactivation mechanisms of *Escherichia coli (E. coli)*.

E. coli contains three types of SOD enzymes with different metal cationic centers: Mn-SOD, Fe-SOD, and Cu Zn-SOD, encoded by genes *sodA*, *sodB*, and *sodC*, respectively. The expression of *sodA* is regulated by the *soxRS* regulon, and is responsible for $^{\bullet}O_2^-$ induction. The expression of gene *sodC* is controlled by another regulator *RpoS* which is related with stationary phase and general stress, and to our knowledge, the regulation of *sodB* gene is not elucidated (Storz et al., 1990; Chiang and Schellhorn, 2012). Similarly, there are two catalases in *E. coli*: hydroperoxidase I (HPI) and hydroperoxidase II (HPII), and they are encoded by *katG* and *katE*, respectively. The gene *katG* is part of the H_2O_2 dependent *oxyR* regulated response system, while the gene *katE* is regulated by *RpoS* independent of H_2O_2 induction (Mukhopadhyay and Schellhorn, 1994; Chiang and Schellhorn, 2012). Thus, the genes *sodA* and *katG* are inducible by $^{\bullet}O_2^-$ and H_2O_2, to produce SOD and catalase, respectively. Therefore, both genes are important for bacterial oxidative stress responses induced by $^{\bullet}O_2^-$ and H_2O_2. Isogenic mutant strains, such as single gene deleted strains (deficient in the gene encoded biofactors), are useful in bacteriology research because they clarify the role of the target biofactors, with the parental strain serving as the control (Nachin et al., 2005). However, only a few studies have applied this method to investigate PC inactivation mechanisms (Gao et al., 2012). Therefore, this study investigates PC and PEC inactivation mechanisms using *E. coli* BW25113 as a parental strain, and its isogenic mutants with the single gene *katG* (*E. coli* JW3914-1) or *sodA* (*E. coli* JW3879-1) deleted. The work focuses on the role of anti-oxidative enzymes, such as catalase and SOD, during the PEC inactivation process. The relationship between ROSs levels, enzyme activities, and PEC inactivation efficiencies will also be assessed. Along with studying PEC-induced bacterial oxidative damages, the PEC inactivation mechanism of *E. coli* will also be explored from the genetic and enzymatic perspective.

2. Experimental section

2.1. Preparation of photoanode and disinfection apparatus setup

All inactivation experiments were performed using a 50-mL three-electrode photoelectrochemical reactor (Fig. 1). The photoanode is a piece of Ti foil with highly oriented TiO_2 nanotubes array at one end (15 mm by 15 mm), which was prepared using anodizing method (Sun et al., 2014). Briefly, Ti foil was pre-anodized for 4 h at 30 V in a mixture of ethylene glycol, 0.5 M HAc, and 0.2 M NH_4F, sonicated in deionized water and anodized for another 24 h at 30 V in the same electrolyte. TiO_2 nanotubes were finally obtained by annealing at 500 °C for 2 h. The counter and reference electrodes are platinum foil and saturated Ag/AgCl, respectively. The LED lamp with a maximum emission at 365 nm and a light intensity adjusted

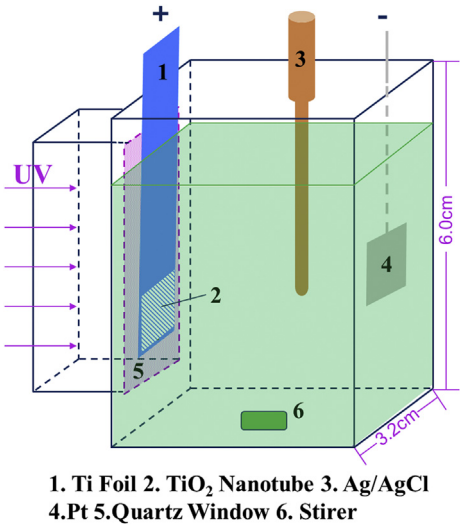

Fig. 1. Schematic diagram of the apparatus used for PEC/PC/EC inactivation of *E. coli*.

to 27 mW cm^{-2} was adopted as a light source. The bias potential of the anode is fixed at 1 V *vs* Ag/AgCl, because the photocurrent of the anode was saturated at this potential and thus the PEC efficiency was maximized (Nie et al., 2013). 0.2 M $NaNO_3$ was used as electrolyte, given that identical concentrations of frequently used electrolyte such as Na_2SO_4 and $NaClO_4$ did not affect the disinfection performance of PEC (Nie et al., 2014).

2.2. E. coli strains and bacterial suspension preparation

The *E. coli* strains used for PEC inactivation were purchased from the Coli Genetic Stock Center (CGSC, Yale University, New Haven, CT, USA) and listed in Table 1. Bacteria incubated overnight in a nutrient broth medium (1% peptone, 0.3% beef extract, 0.5% NaCl, pH 7.4) were diluted with fresh autoclaved nutrient broth at 1/100, and incubated at 37 °C and 200 rpm. Absorbance at 600 nm was measured at set intervals to establish a bacterial growth curve. The bacterial suspension was centrifuged at 10,000 rpm for 2 min, washed twice with sterilized water, and re-suspended in 0.2 M $NaNO_3$ for PEC inactivation. The initial *E. coli* density was ~2×10^7 colony forming units per milliliter (CFU mL^{-1}).

2.3. Inactivation kinetics

Fifty milliliters of prepared *E. coli* suspension was inactivated using PEC, PC, or electrochemistry (EC). The cell viabilities were estimated by means of colony-counting procedure after series of dilution with sterile water (Shi et al., 2014). The inactivation curves were fitted using a predefined model (Geeraerd et al., 2000: Log-Linear + Shoulder + Tail) (Geeraerd et al., 2000) using the GInaFIT tool in Microsoft Excel 2010 (version 1.6, accessed at http://cit.kuleuven.be/biotec/ginafit.php in June 2014) (Geeraerd et al., 2005). The inactivation curves included three stages: (1) the shoulder, the initial delay phase; (2) the log phase, when bacteria show fast inactivation; (3) the tail, when inactivation is decelerated. After fitting, three kinetic parameters are acquired, corresponding to the three stages: SL (shoulder length, min), k_{max} (slope of the curve at stage 2, CFU mL^{-1} per min), and $logN_{res}$ (starting point of the tail, CFU mL^{-1}).

Table 1
E. coli strains.

Biotic factor	Strain name	CGSC[a] no.	Mutation name	Gene deletion	Gene function
Parental strain	BW25113	7636	None	None	None
SOD	JW3879-1	10798	sodA768(del)::kan	sodA	Mn-SOD
Catalase	JW3914-1	10827	katG729(del)::kan	katG	Catalase HPI

[a] CGSC = Coli Genetic Stock Center, Yale University.

2.4. ROSs detection and the enzymatic activities assay

The concentrations of extracellular ROSs, including H_2O_2, $^{\bullet}OH$, and $^1O_2$ in the inactivation systems were monitored. [H_2O_2] was measured based on the decolonization of methyl orange caused by $^{\bullet}OH$ oxidation generated from Fenton reaction (Luo et al., 2008). Briefly, 1.8 mL of samples were mixed with 0.2 mL 100 mg L^{-1} methyl orange, and the pH was adjusted to 2.5 with 0.1 M H_2SO_4. The reaction was started by adding 20 μL 0.05 M $FeSO_4$. The absorbance at 507 nm ($A_{507\ nm}$) was recorded at 0 and 2 min, respectively. [H_2O_2] was linear correlated with the decrease of $A_{507\ nm}$ ($\Delta A_{507\ nm}$). Steady state $^{\bullet}OH$ concentration ([$^{\bullet}OH$]ss) was determined using *p*-chlorobenzoic acid (*p*CBA) as probe as follows (Cho et al., 2004):

$$-d[p\mathrm{CBA}]/dt = k_{exp}[p\mathrm{CBA}] = k_{\bullet OH,p\mathrm{CBA}}[^{\bullet}OH]_{s.s.}[p\mathrm{CBA}] \quad (1)$$

$$-\ln([p\mathrm{CBA}]/[p\mathrm{CBA}]_0) = k_{exp}t \quad (2)$$

$$k_{exp} = k_{\bullet OH,p\mathrm{CBA}}[^{\bullet}OH]_{s.s.} \quad (3)$$

Given that $k_{\bullet OH,p\mathrm{CBA}} = 5 \times 10^9\ M^{-1}\ s^{-1}$, $[^{\bullet}OH]_{s.s.}$ can be calculated. [*p*CBA] was monitored at 240 nm by HPLC equipped with a DIKMA C18 column (250 mm × 4.6 mm × 5 μm). The mobile phase was acetonitrile:0.1% phosphoric acid = 55:45 at 0.8 mL min^{-1}. $[p\mathrm{CBA}]_0$ was 20 μM.

[$^1O_2$] was monitored by furfuryl alcohol (FFA), and the calculation was as follows:

$$-\ln([\mathrm{FFA}]/[\mathrm{FFA}]_0) = k_{exp}t \quad (4)$$

$$k_{exp} = k(\mathrm{FFA}, {}^1O_2)[{}^1O_2] \quad (5)$$

$k(\mathrm{FFA}, {}^1O_2) = 1.2 \times 10^8\ M^{-1}\ s^{-1}$, and [FFA] was determined by HPLC at 218 nm, and the mobile phase was methanol:H_2O = 20:80 at 0.8 mL min^{-1}.

The intracellular ROSs level in *E. coli* cells (mainly $^{\bullet}OH$ and H_2O_2) was tested with a fluorescent probe 2′,7′-dichlorodihydrofluorescein diacetate (DCFH-DA) (Royall and Ischiropoulos, 1993; Rohnstock and Lehmann, 2007). Five milliliters of bacteria was withdrawn from the disinfection system and mixed with 5 μL DCFH-DA (1 mM) immediately. After incubated at 37 °C for 20 min in dark, the suspension was concentrated with tubular ultrafiltration modules (Amicon® Ultra-4 10K, Millipore) to a final volume of 200 μL and pipetted into a microplate for fluorescent measurement at 525 nm with excitation at 488 nm.

For catalase and SOD activities, eight milliliters of *E. coli* suspension was filtered through 0.22 μm filters (SCBB-207, Shanghai ANPEL Scientific Instrument Co., Ltd., China) to harvest the cells and lysed using 100 μL of B-PER® Bacterial Protein Extraction Reagent (Pierce Biotechnology, USA). The lysate was centrifuged at 10,000 rpm for 1 min, and the supernatant was ready for catalase and SOD activity assays using Catalase Assay Kit (S0051, Beyotime Institute of Biotechnology, China) and Superoxide Dismutase Assay Kit (Item No. 706002, Cayman Chemical, USA), respectively, following the manufacturer's instruction.

2.5. H_2O_2 pre-incubation

Bacteria incubated overnight were diluted with fresh nutrient to $OD_{600\ nm} = 0.035$, and H_2O_2 were added to final concentrations of 0, 30, 100, 200, 500 μM for pre-incubation. The suspension was incubated at 37 °C and 200 rpm for 70 min, and determined catalase activities. The pre-incubated bacteria were harvested and resuspended in 0.2 M $NaNO_3$ to a cell density of ~5×10^5 CFU mL^{-1} for PEC inactivation.

2.6. Bacterial oxidative damage detection

For the K^+ leakage analysis, the *E. coli* suspension was filtered with 0.22 μm filter after PEC inactivation to remove bacterial cells. The filtrate was tested for K^+ concentration using inductively coupled plasma-atomic emission spectroscopy (VARIAN VISTA ICP-AES Pro, USA) at 766.5 nm.

For the SEM analysis, the harvested cells was fixed with 2.5% glutaraldehyde overnight, and then washed them with 0.1% phosphate-buffered saline five times, each for 20 min. Samples were dehydrated with 30, 50, 70, 90 and 100% ethanol, and 100% butyl alcohol, successively. The samples were freeze dried and gold sputter coated before being imaged with a Field Emission Scanning Electron Microscope (FESEM, JSM-6330F, JEOL Ltd., Japan) (Li et al., 2013).

For the protein carbonyl assay, *E. coli* (10^8 CFU mL^{-1}) was lysed by sonication after PEC inactivation with 50 μL 100 mM Phenylmethanesulfonyl fluoride and 5 μL 5% butylated hydroxytoluene. Then, the protein concentration in the lysate was adjusted to 10 μg mL^{-1}, and the protein carbonyl concentration using an Oxi-Select Protein Carbonyl ELISA Kit (STA-310, Cell Biolabs, USA), following the manufacturer protocol. The protein concentration of the lysate was determined using a Bradford assay (SK3041, Sangon Biotech, Shanghai, China).

For the cell viability assay, bacterial viability was tested using a LIVE/DEAD® BacLight Bacterial Viability Kit (Molecular Probes, USA) with a fluorescence microplate reader. The excitation wavelength was 485 nm, and the fluorescence intensity at both 530 and 630 nm were measured simultaneously. The calibration curve was obtained using mixed suspensions of permeabilized and intact bacteria at different ratios. Detailed methods can be found in the assay protocols provided by the manufacturer.

2.7. Statistical analysis

Statistical significance was determined using the Student two-tail *t* test, and the homogeneity of variance was checked by F test. The One-Way ANOVA was used for multiple comparisons. Differences between groups were considered significant if $p \leq 0.05$.

3. Results and discussion

3.1. Influence of growth phase on PEC inactivation performance

Fig. S1 shows *E. coli* strain growth curves. Similar growth curves were observed for three strains, that is, the bacterial growth entered log phase at ~2 h and the stationary phase at ~13 h. That said, the *katG*$^-$ mutant cell density was lower than that of the parental strain BW25113. This may be due to the deficient catalase HPI and higher ROSs level, which subsequently accumulated in *katG*$^-$ mutant cells (GonzalezFlecha and Demple, 1997). As such, the catalase and SOD activities of the strains were evaluated throughout the bacterial growth period (Fig. 2). Enzyme activities were normalized by relative cell density, with the unit density set at $OD_{600\ nm} = 1$. The relative cell density was plotted against the $OD_{600\ nm}$ of the bacterial suspension; linear correlation was achieved within appropriate OD intervals (Fig. S2), allowing the relative bacterial density to be calculated from the $OD_{600\ nm}$ of the suspension.

As Fig. 2 shows, for BW25113, catalase and SOD activities started to rise after 2 h (early-log phase), peaked at 6 h (mid-log phase), and then decreased thereafter. The bacterial anti-oxidative enzymes level reflected the management of bacteria to the oxidative stress. The use of oxygen by bacteria through aerobic respiration generates ROSs such as $^{\bullet}O_2^-$ and H_2O_2 as by-products (Chiang and Schellhorn, 2012) Low H_2O_2 concentration in bacterial cells (less than 0.7 μM) is necessary for cellular signal conduction (Stone and Yang, 2006), but higher ROSs levels will pose oxidative stress to bacteria. Bacterial responses, such as elevated catalase and SOD, are induced to scavenge the ROSs and prevent oxidative damages. The ROSs level in the lag phase was low because of small cell density and slow metabolism at this stage; the catalase and SOD level was correspondingly low.

After entering the log phase, the rapid metabolism and division of cells increased the ROSs level. Other studies suggest that in log phase, the H_2O_2 production rate is more than 10 times higher than in the lag phase (GonzalezFlecha and Demple, 1997), inducing catalase and SOD. Nevertheless, both enzyme activities in the stationary phase declined due to the decreased metabolism rate. Compared with BW25113, *sodA*$^-$ mutant showed significantly lower SOD activity due to gene deletion of *sodA* (encoding Mn-SOD), whereas the catalase levels of *katG*$^-$ (encoding catalase HPI) mutant were significantly lower after 8 h of incubation (Fig. 2, $P \leq 0.05$). The results confirmed the gene functions of *sodA* and *katG* which was deleted in our target mutant strains, and facilitated the following investigations of bactericidal ROSs and bacterial responses to oxidative stress during PEC inactivation.

PEC inactivation of *E. coli* BW25113 at different phases was further investigated to investigate phase-related anti-oxidative enzymatic activities. As Fig. 3a shows, the bacteria at early log phase (3 h) were the most sensitive to PEC inactivation, whereas the bacteria at the mid-log phase were the most insusceptible. The sensitivity to PEC rose again during 12–16 h point (Fig. 3b). Considering catalase and SOD levels in Fig. 2, bacteria with higher enzymatic activities are clearly more resistant to PEC treatment. However, when the bacteria entered the late stationary phase (after 16 h), the time needed to fully inactivating bacteria increased over a longer growing time (Fig. 3b). It may be that at the stationary phase, with exhausted nutrients and accumulated hazardous metabolites,

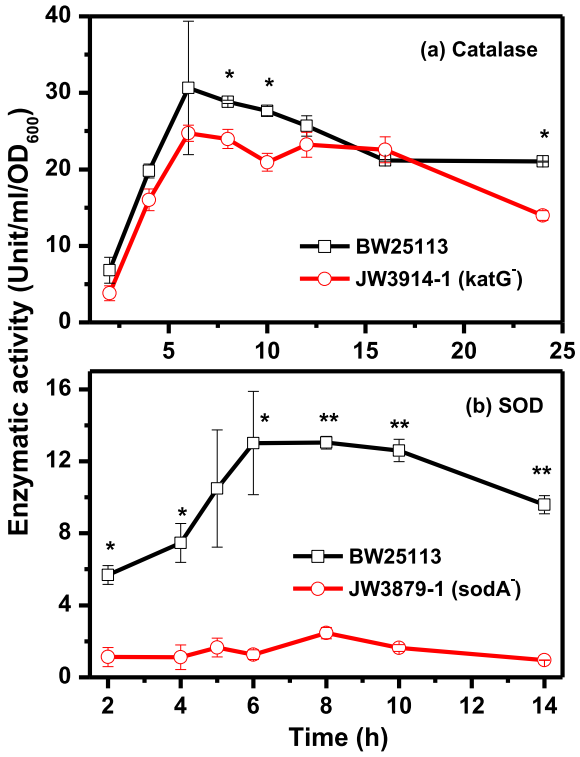

Fig. 2. Enzymatic activities evolution of (a) catalase and (b) SOD throughout the bacterial growth. Data expressed as mean ± standard deviation (SD); bars, SD; n = 3. * ($P \leq 0.05$) and ** ($P \leq 0.01$) indicate the significance levels determined by Student's *t* test.

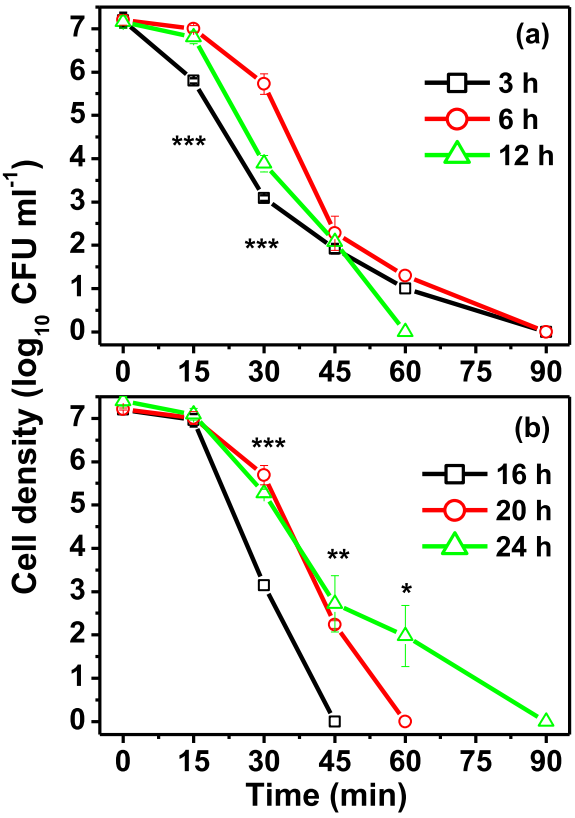

Fig. 3. PEC inactivation performance of *E. coli* BW25113 at various growing phases. Data expressed as mean ± standard deviation (SD); bars, SD; n = 3. * ($P \leq 0.05$), ** ($P \leq 0.01$) and *** ($P \leq 0.001$) indicate the significance levels determined by One-Way ANOVA.

various bacterial responses are induced, including smaller and rounder cell morphology, smaller DNA (Chung et al., 2006), and increased DNA binding protein (Dps) expression (Calhoun and Kwon, 2011) resulting in stronger anti-oxidative capacity.

For the parental strain and mutants, the PEC inactivation efficiency of *E. coli* at mid-log phase is the greatest for the mutant *katG*$^-$ followed by the mutant *sodA*$^-$, and then strain BW25113 (Fig. 4). For instance, after 30 min of PEC inactivation, the survived bacteria were (3.43 ± 0.49) log for the mutant *katG*$^-$, (4.34 ± 0.34) log for the mutant *sodA*$^-$, and (5.72 ± 0.24) log for the parental strain ($P < 0.05$, One-Way ANOVA). With higher catalase and SOD activities of BW25113, we infer that both enzymes, especially catalase, play an important role in the bacterial defense against PEC inactivation. Correspondingly, the catalase substrate, H_2O_2, should be the dominant bactericide in the PEC process. Compared with PEC, neither PC nor EC showed effective inactivation to all three strains during the entire 90 min inactivation process (Fig. S3), which was different from the vastly reported PC inactivation performance of TiO_2/UV system. This can be due to the immobilized catalyst, small catalyst area (15 mm × 15 mm) and the large inactivation volume (50 mL bacterial suspension), which resulted in the far more limited contact between catalyst and bacteria, compared with the suspended TiO_2 system. In fact, the BW25113 can be inactivated by PC when using a thin layer reactor (100 μL) in our previous report, where the same anode and UV were adopted (Nie et al., 2014). Nevertheless, the poor performance of PC also indicated that the PEC inactivation mechanism was independent of the close contact between catalyst and bacteria, differing from routine TiO_2/UV systems.

3.2. Mode of action: how does catalase affect PEC inactivation?

To confirm our inferences about the role of catalase and H_2O_2 in PEC inactivation process, the concentrations of various extracellular ROSs, including H_2O_2, $^{\bullet}OH$ and $^1O_2$ were measured. Results are shown in Fig. 5a ($[H_2O_2]$) and Table S1 ($[^{\bullet}OH]_{s.s.}$ and $[^1O_2]$). In PEC system without bacteria, the $[H_2O_2]$ increased as soon as the reaction started, and the saturated $[H_2O_2]$ of ~28 μM was reached within 60 min. However, the $[H_2O_2]$ in PC or EC showed little increase. In our previous report, the ROSs scavenging experiments with the same PEC experimental apparatus showed that the bactericidal ROSs were found to be dominantly generated from

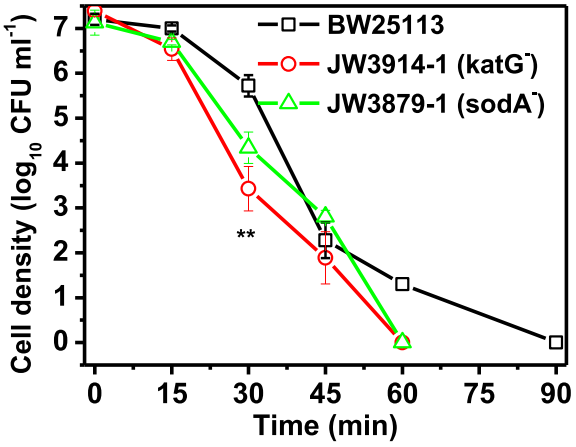

Fig. 4. PEC inactivation efficiency of *E. coli* BW25113 and isogenic mutant strains *katG*$^-$, *sodA*$^-$ in mid-log phase. Data expressed as mean ± standard deviation (SD); bars, SD; n = 3. ** ($P \leq 0.01$) indicate the significant level determined by One-Way ANOVA.

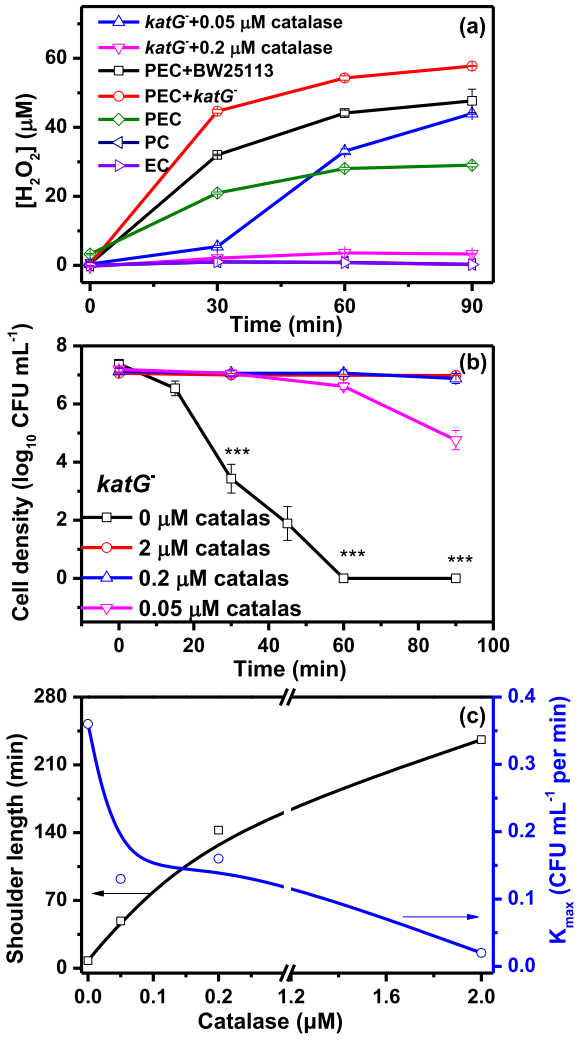

Fig. 5. (a) H_2O_2 concentration measurement in PEC inactivation systems. PEC, PC, and EC experiments were conducted in 0.2 M $NaNO_3$ without *E. coli* as the control. PEC + BW25113 and PEC + *katG*$^-$ mean PEC disinfection system with BW25113 and *katG*$^-$, respectively. *katG*$^-$ + catalase represents PEC disinfection of *katG*$^-$ with catalase added; (b) The PEC inactivation performance of *katG*$^-$ strain with catalase added at various concentrations; (c) The correlation between the inactivation kinetic parameters and the catalase concentration added in PEC + *katG*$^-$ system, and the arrows indicate the corresponding axes. Data expressed as mean ± standard deviation (SD); bars, SD; n = 3. *** ($P \leq 0.001$) indicates the significant level determined by One-Way ANOVA.

valence band (Sun et al., 2014). Therefore, the H_2O_2 was suggested to be formed through the following reactions (Equations (6)–(8)):

$$TiO_2 + h\nu \rightarrow e^- + h^+ \quad (6)$$

$$h^+ + H_2O \rightarrow {}^{\bullet}OH + H^+ \quad (7)$$

$$2{}^{\bullet}OH \rightarrow H_2O_2 \quad (8)$$

where *hv* referred to the UV irradiation, e^- was the free electrons in conduction band, and h^+ was the holes in valence band. The $[H_2O_2]$ in PC did not show obvious increase due to the limited catalyst area and the large bulk volume as mentioned, as well as the fast recombination of h^+ and e^-. In PEC, the recombination was effectively suppressed by the bias potential, and the reactions in Equations (2) and (3) were elevated greatly, resulting into the

significantly increased [H_2O_2].

The contribution of H_2O_2 to PEC inactivation was further demonstrated. The [H_2O_2] in PEC system with *katG*$^-$ mutant was ~10 μM higher than that with BW25113 (Fig. 5a). Furthermore, Adding catalase can scavenge H_2O_2 effectively; 0.05 and 0.2 μM catalase prevented the rise of [H_2O_2] in the first 30 and 90 min, respectively, despite the gradually inactivation of catalase by PEC (Fig. S4). Correspondingly, the PEC inactivation efficiency was decreased significantly by the catalase addition (Fig. 5b). The PEC inactivation curves were fitted using GInaFIT, and the kinetic parameters (SL and k_{max}) were plotted against the catalase concentration (Fig. 5c). Adding catalase to PEC system increased the shoulder length and decreased the slope of PEC inactivation curve simultaneously. The PEC inactivation efficiency of *katG*$^-$ + catalase was even lower compared that of BW25113, due to much lower [H_2O_2] of *katG*$^-$ + catalase than BW25113 (Fig. 5a), caused by higher catalase activity of *katG*$^-$ + catalase systems than BW25113 (data shown later in Section 3.4). The profiles of [H_2O_2] coincided with the inactivation performance, which supported our assumption of the dominant role of H_2O_2 in PEC inactivation. While in the report of Wang et al. (2011), direct addition of H_2O_2 with similar concentration (5 μM) did not show any elevated disinfection effect. Nevertheless, continuous addition of H_2O_2 with this concentration did inactivate the bacteria slowly. Thus the author suggested that in PC disinfection system, the actual amount of H_2O_2 available to attack bacteria was much more than the amount detected because H_2O_2 was continuously consumed by both bacterial cells attacking and the decomposition. Therefore, in the present PEC system, the continuously generated large amount of H_2O_2 was responsible for the bacterial inactivation.

In addition, the [$^{\bullet}$OH] decreased in the order of PEC, PC and EC, and [$^1O_2$] was almost the same in all three systems (Table S1). The profiles of [$^{\bullet}$OH] and [$^1O_2$] were inconsistent with the disinfection performance, suggesting that neither of them was the major bactericide. The conclusion was supported by the ROSs scavenging experiments in our early report (Sun et al., 2014), where the PEC disinfection efficiency just decreased slightly after $^{\bullet}$OH and O_2 were quenched. The conclusion seemed conflict with the common sense that $^{\bullet}$OH rather than H_2O_2 was responsible for bactericidal effect because it's more reactive. In fact, in this study, the bacteria-catalyst contact was insufficient, thus the bactericidal effect of $^{\bullet}$OH was limited by its short life-span (~300–500 μs) because it's generally produced on the catalyst surface. On the contrary, the H_2O_2 formed on the anode in PEC system could diffuse into the bulk bacterial suspension, and also transport across the bacterial membrane and subsequently transform into $^{\bullet}$OH through Fenton or Harbor–Weiss reaction inside the cell (Kikuchi et al., 1997; Gogniat and Dukan, 2007). Thus, the inactivation of bacteria can be caused by both extracellular H_2O_2 and its intracellular derivative $^{\bullet}$OH.

3.3. H_2O_2 pre-incubation elevated bacterial resistance to PEC

Studies have shown that bacteria pre-treated with a non-lethal dose of H_2O_2 show reduced sensitivity to lethal doses of H_2O_2 (Imlay and Linn, 1986). Given that the dominant ROS in the PEC process was H_2O_2, the pre-treatment was conducted before PEC inactivation (Fig. 6). The catalase activity of *E. coli* BW25113 after H_2O_2 pre-incubation increased in a [H_2O_2] dependent manner, whereas the catalase in the *katG*$^-$ strain was not induced (Fig. 6a). This result further confirmed that catalase HPI encoded by the *katG* gene was H_2O_2 inducible (Storz et al., 1990), while the catalase HPII encoded by *katE* was H_2O_2 independent. For BW25113, the resistance to PEC inactivation increased after H_2O_2 pre-incubation; higher [H_2O_2] resulted in more resistant bacteria (Fig. 6b). The inactivation curves were fitted using GInaFIT; kinetic parameters SL and k_{max} are also listed in Table 2. It was found that H_2O_2 pre-incubation affected SL rather than k_{max}. When the SL was plotted against the catalase level, a good positive linear relationship was obtained, with $R^2 = 0.9612$ (Fig. S5). In contrast, in the catalase HPI deficient strain *katG*$^-$, H_2O_2 pre-incubation elevated neither the catalase level nor PEC insusceptibility. Although H_2O_2 can induce expression of various proteins that protect the cells, such as alkyl hydroperoxidase, while the different responses of the parental

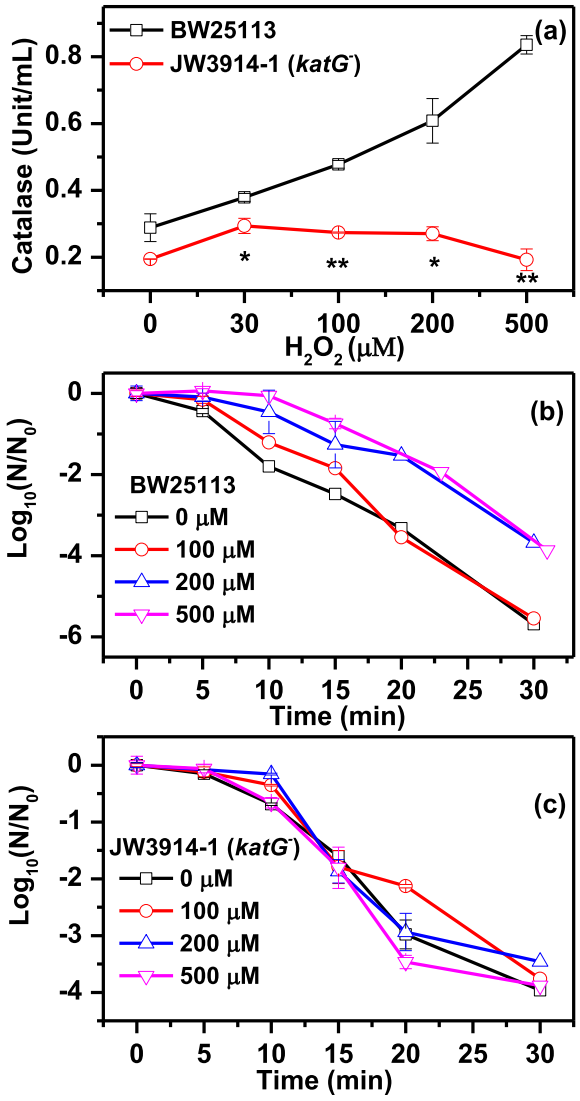

Fig. 6. (a) Catalase activity of *E. coli* after pre-incubation with various H_2O_2 levels; PEC inactivation performance with H_2O_2 pre-incubated, (b) BW25113 strain and (c) *katG*$^-$ strain. Data expressed as mean ± standard deviation (SD); bars, SD; n = 3. * ($P \leq 0.05$) and ** ($P \leq 0.01$) indicate the significant levels determined by Student's *t* test.

Table 2
Catalase levels and PEC inactivation kinetic parameters[a] of *E. coli* BW25113 pre-incubated with various doses of H_2O_2.

H_2O_2 (μM)	0	100	200	500
Catalase (Unit mL^{-1})	0.29	0.48	0.61	0.84
Sl (Shoulder length, min)	2.46	5.99	9.16	11.18
k_{max} (CFU mL^{-1} min^{-1})	0.47	0.56	0.39	0.49

[a] Fitted with GInaFIT.

strain and the *katG* mutant could provide solid evidences to reach the conclusion. That is, enhanced bacterial resistance to PEC inactivation by H_2O_2 pre-incubation was probably attributed to the induction of catalase HPI.

3.4. Oxidative stress responses of E. coli to PEC treatment

Given the important role of H_2O_2 in PEC inactivation, the intracellular ROSs and catalase levels were also monitored during the PEC inactivation process to assess whether the oxidative stress responses were induced by PEC treatment, such as H_2O_2 pre-incubation. As Fig. 7a shows, the intracellular ROSs level continuously increased in the initial 30 min; the level in PEC + *katG*$^-$ system was higher than in the PEC + BW25113 system. Trends for intracellular ROSs levels (monitored by DCFH-DA) were similar to trends for extracellular [H_2O_2]. This supported our hypothesis that the exogenous H_2O_2 in PEC system could diffuse across the bacterial membrane and transform into more reactive $^{\bullet}OH$ through a Fenton or Harbor–Weiss reaction inside the cell (Sun et al., 2014). The decrease of fluorescent intensity after 30 min of PEC may be due to the leakage of DCFH-DA endogenous fluorescent product, caused by increased membrane permeability. The catalase and SOD levels in the parent and deficient mutants decreased gradually during the PEC inactivation process (Fig. 7b and c), suggesting that enzymes were not induced by the elevated intracellular ROSs level during PEC inactivation process. It may be that the oxidative stress in PEC system overwhelmed the defensive capacity of *E. coli*, or that there were insufficient nutrients for oxidative responses such as anti-oxidative enzyme synthesis (e.g. catalase and SOD). Besides, the initial catalase activity of BW25113 (0.2 Unit mL^{-1}, Fig. 7b) was much lower than that added *katG*$^-$ (37.7 and 10.8 Unit mL^{-1} for 0.2 and 0.05 μM catalase, Fig. S4), explaining the reason why lower [H_2O_2] and disinfection efficiency of *katG*$^-$ + catalase than BW25113 were obtained during PEC treatment (Fig. 5).

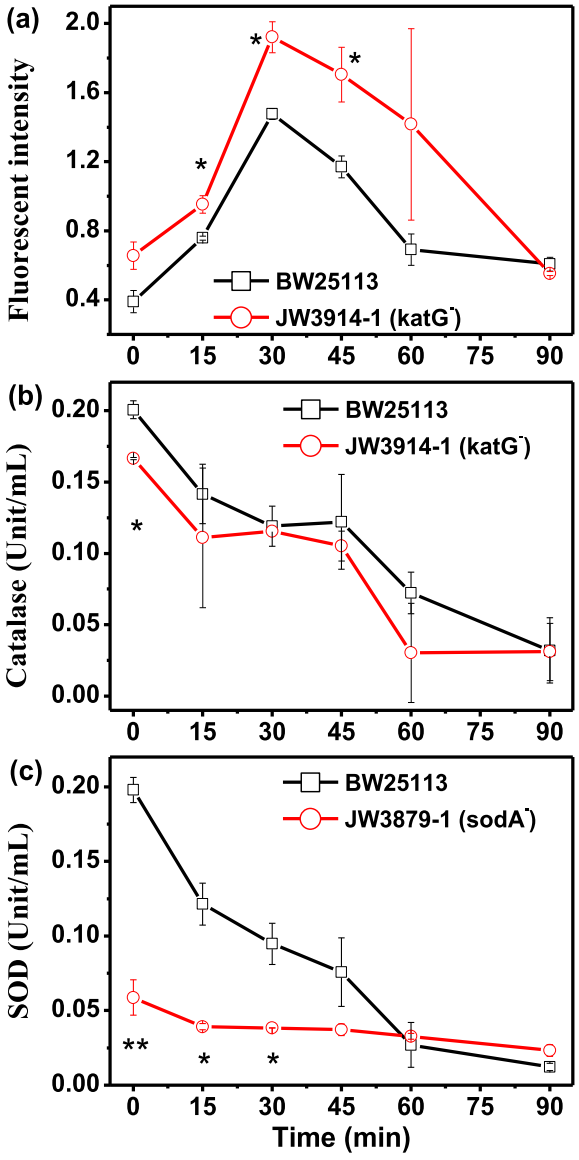

Fig. 7. (a) The intracellular ROSs level tested by DCFH-DA; (b) catalase activity and (c) SOD activity of three *E. coli* strains during PEC inactivation process. Data expressed as mean ± standard deviation (SD); bars, SD; n = 3. * ($P \leq 0.05$) and ** ($P \leq 0.01$) indicate the significant levels determined by Student's *t* test.

3.5. Oxidative damages of E. coli caused by PEC treatment

The invalidation of the *E. coli* defensive system against the oxidative stress results in ROSs accumulation in bacterial cells, attacking cellular components and leading to further oxidative damages. The bacterial envelope, composed of the outer membrane, the peptidoglycan layer, and the cytoplasmic membrane, had the greatest probability of being exposed to ROSs attack compared with other cellular components in the PEC system. The functional or structural disruption of the membrane generally increases the permeability, which can be monitored by the leakage of cytoplasmic K^+. K^+ is important for bacterial cells to retain the resting potential, for balancing osmotic pressure, and conducting signals. Intact bacterial cells maintain intracellular [K^+] at a higher level than the extracellular surroundings through a Na^+–K^+ pump (Wang and O'Doherty, 2012). As Fig. 8 shows, compared with the negative control experiments (the same bacterial suspension as in the PEC experiments stirred in the dark without the catalyst in triangular flasks), the [K^+] in extracellular solution increased gradually during PEC inactivation, indicating the elevated permeability of the bacterial membrane. The K^+ leakage may be due to the inactivation of energy metabolism associated enzymes such as ATPase, and the subsequent loss of membrane potential. This

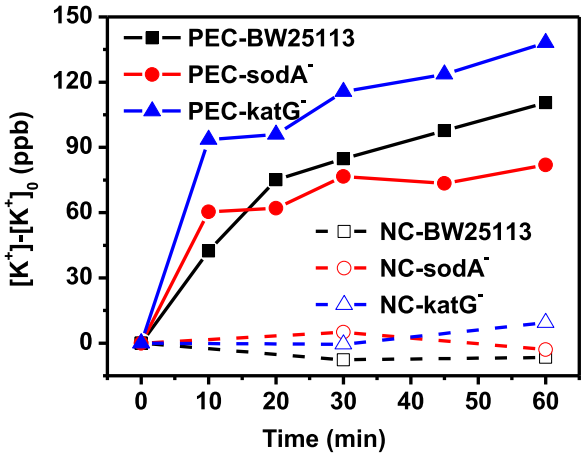

Fig. 8. Leakage of K^+ in PEC inactivation experiments with parental *E. coli* and its isogenic mutant strains *sodA*$^-$ and *katG*$^-$ (NC: negative control; PEC: photoelectrocatalysis).

potential is important for transporting various substrate across the membrane (Bosshard et al., 2010). Besides the functional disruption of the bacterial membrane, structural damage like lipid peroxidation caused by the ROSs attack may be responsible for the increased membrane permeability (Carre et al., 2014). Compared with the mutants, BW25113 showed slower K^+ leakage. For instance, after 10 min of PEC inactivation, the leaked K^+ concentration was 38% of the maximum (reached at 60 min) for BW25113; whereas the concentration was 74% for *sodA*$^-$ and 68% for *katG*$^-$, respectively. Thus, it can be inferred that catalase and SOD can protect the membrane from ROSs attack to some extent, and the permeabilized membrane is partly responsible for bacterial death.

To further investigate bacterial envelope damage, we used FESEM to image the PEC-treated bacterial samples of the three strains; Fig. 9 shows the representative images. These figures clearly show that PEC inactivation causes time-dependent damage to the bacterial envelope. For BW25113, the untreated cells showed a solid rod shape with a smooth surface. After 60 min of PEC treatment, some cells exhibited a collapsed appearance; the number of collapsed cells increased up to the 90 min point. When PEC treatment was prolonged to 120 min, even more severely damaged cells were observed with obviously broken envelopes. Both mutants (*katG*$^-$ and *sodA*$^-$) showed faster and more severe damage than BW25113, even with the same PEC treatment interval. In particular, cell debris was observed at the 90 min point for both mutants, but not for the parental strain.

Protein is the major building block of bacterial cells. An ROSs attack generally causes oxidative damage to bacterial cell proteins. Protein carbonyl is usually detected as a bio-marker of the oxidized proteins, because it is widely generated and relatively stable for detection (Dalle-Donne et al., 2003). Fig. 10 shows the protein carbonyl levels of the parental strain and two mutants during PEC treatment. To acquire sufficient protein for the assay, bacterial suspension of approximately 10^8 CFU mL^{-1} was used for PEC inactivation. Fig. S6 illustrates the bacterial viability and the protein concentrations of the harvested bacterial lysate.

After 3 h of PEC treatment, more than 99% of the bacteria were inactivated (Fig. S6a), and the protein concentration showed a time-dependent decrease (Fig. S6b). This may be due to membrane protein loss and cytoplasm leakage. The protein carbonyl concentration increased with PEC treatment time, particularly after 1.5 h (Fig. 10). In addition, the *katG*$^-$ mutant exhibited significantly earlier and faster increase in the protein carbonyl levels compared with strain BW25113 ($P \leq 0.05$), suggesting that H_2O_2 and its intracellular derivative $^{\bullet}OH$ are the major ROSs causing protein oxidation, and that catalase can efficiently prevent oxidative damage to the bacterial protein. Therefore, the lower protein carbonyl level before the 1.5 h point may be explained by the preservation of relatively higher catalase activity. The elevated carbonyl concentration may be due to the compromised catalase activity or SOD. The decrease of carbonyl concentration after 4 h may be due to the further degradation of the oxidized proteins

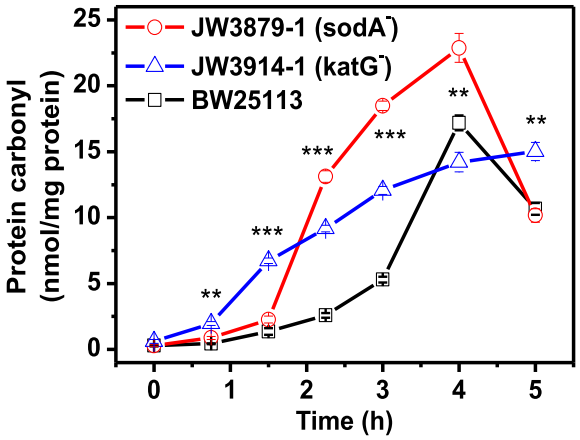

Fig. 10. Protein carbonyl concentration of bacterial samples (~10^8 CFU mL^{-1}) after PEC treatment at different intervals. Data expressed as mean ± standard deviation (SD); bars, SD; n = 3. ** ($P \leq 0.01$) and *** ($P \leq 0.001$) indicate the significant levels determined by One-Way ANOVA.

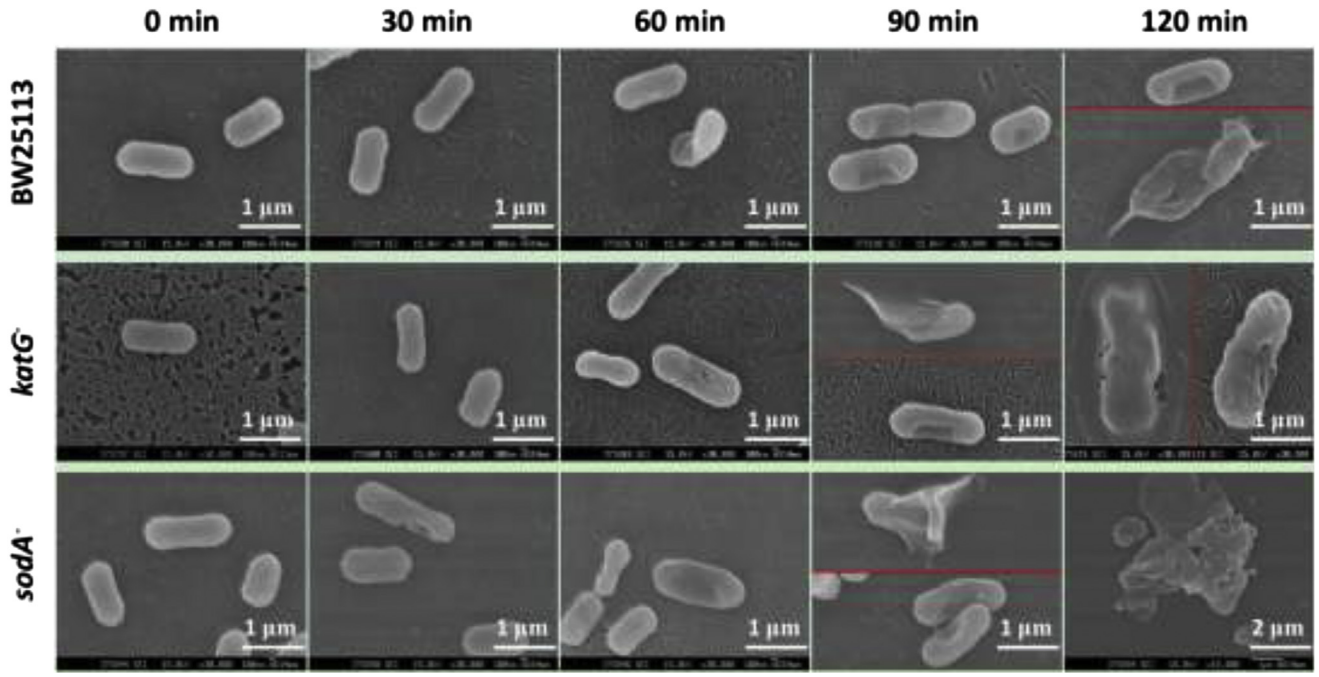

Fig. 9. The SEM images of three strains of *E. coli* after being treated by PEC inactivation.

considering that PEC was able to degrade organic matter (e.g., cellular components and inactivated bacteria) and inactivate bacteria simultaneously (Li et al., 2011).

4. Conclusions

It was found that H_2O_2 was the major extracellular bactericide generated during the PEC inactivation, where direct contact between catalyst and bacteria was insufficient for short-life ROSs such as $^{\bullet}OH$. Nevertheless, $^{\bullet}OH$ might be derived from the permeated H_2O_2 inside the cells. Catalase, which quenched H_2O_2, contributed greatly to the bacterial resistance to PEC. The *E. coli* catalase level affected PEC inactivation significantly, in particular the shoulder length of inactivation curves. SOD was another important defensive enzyme, as the strain deficient in SOD was also more susceptible to PEC inactivation than the parental strain. Both enzymes can protect the bacterial cells to some extend from oxidative damages such as membrane decomposition, cytoplasm leakage and protein carbonyl.

Acknowledgments

This is contribution No. IS–2135 from GIGCAS. This work was supported by National Natural Science Foundation of China (41573086), National Natural Science Funds for Distinguished Young Scholars (41425015), Research Grant Council, Hong Kong SAR Government (GRF476811).

Appendix A. Supplementary data

Supplementary data related to this article can be found at http://dx.doi.org/10.1016/j.watres.2015.10.003.

References

Baram, N., Starosvetsky, D., Starosvetsky, J., Epshtein, M., Armon, R., Ein-Eli, Y., 2007. Enhanced photo-efficiency of immobilized TiO_2 catalyst via intense anodic bias. Electrochem. Commun. 9, 1684–1688.

Bosshard, F., Bucheli, M., Meur, Y., Egli, T., 2010. The respiratory chain is the cell's Achilles' heel during UVA inactivation in *Escherichia coli*. Microbiology 156, 2006–2015.

Calhoun, L.N., Kwon, Y.M., 2011. Structure, function and regulation of the DNA-binding protein Dps and its role in acid and oxidative stress resistance in *Escherichia coli*: a review. J. Appl. Microbiol. 110, 375–386.

Carre, G., Hamon, E., Ennahar, S., Estner, M., Lett, M.C., Horvatovich, P., Gies, J.P., Keller, V., Keller, N., Andre, P., 2014. TiO_2 photocatalysis damages lipids and proteins in *Escherichia coli*. Appl. Environ. Microbiol. 80, 2573–2581.

Chiang, S.M., Schellhorn, H.E., 2012. Regulators of oxidative stress response genes in *Escherichia coli* and their functional conservation in bacteria. Arch. Biochem. Biophys. 525, 161–169.

Cho, M., Chung, H., Choi, W., Yoon, J., 2004. Linear correlation between inactivation of *E-coli* and OH radical concentration in TiO_2 photocatalytic disinfection. Water Res. 38, 1069–1077.

Chung, H.J., Bang, W., Drake, M.A., 2006. Stress response of *Escherichia coli*. Compr. Rev. Food Sci. Food Saf. 5, 52–64.

Dalle-Donne, I., Rossi, R., Giustarini, D., Milzani, A., Colombo, R., 2003. Protein carbonyl groups as biomarkers of oxidative stress. Clin. Chim. Acta 329, 23–38.

Dalrymple, O.K., Stefanakos, E., Trotz, M.A., Goswami, D.Y., 2010. A review of the mechanisms and modeling of photocatalytic disinfection. Appl. Catal. B Environ. 98, 27–38.

Foster, H.A., Ditta, I.B., Varghese, S., Steele, A., 2011. Photocatalytic disinfection using titanium dioxide: spectrum and mechanism of antimicrobial activity. Appl. Microbiol. Biotechnol. 90, 1847–1868.

Gao, M.H., An, T.C., Li, G.Y., Nie, X., Yip, H.Y., Zhao, H., Wong, P.K., 2012. Genetic studies of the role of fatty acid and coenzyme A in photocatalytic inactivation of *Escherichia coli*. Water Res. 46, 3951–3957.

Gao, P., Liu, J., Sun, D.D., Ng, W., 2013. Graphene oxide-CdS composite with high photocatalytic degradation and disinfection activities under visible light irradiation. J. Hazard. Mater. 250, 412–420.

Geeraerd, A.H., Herremans, C.H., Van Impe, J.F., 2000. Structural model requirements to describe microbial inactivation during a mild heat treatment. Int. J. Food Microbiol. 59, 185–209.

Geeraerd, A.H., Valdramidis, V.P., Van Impe, J.F., 2005. GInaFiT, a freeware tool to assess non-log-linear microbial survivor curves. Int. J. Food Microbiol. 102, 95–105.

Gogniat, G., Dukan, S., 2007. TiO_2 photocatalysis causes DNA damage via fenton reaction-generated hydroxyl radicals during the recovery period. Appl. Environ. Microbiol. 73, 7740–7743.

GonzalezFlecha, B., Demple, B., 1997. Homeostatic regulation of intracellular hydrogen peroxide concentration in aerobically growing *Escherichia coli*. J. Bacteriol. 179, 382–388.

Imlay, J.A., Linn, S., 1986. Bimodal pattern of killing of DNA-repair-defective or anoxically grown *Escherichia-coli* by hydrogen-peroxide. J. Bacteriol. 166, 519–527.

Kikuchi, Y., Sunada, K., Iyoda, T., Hashimoto, K., Fujishima, A., 1997. Photocatalytic bactericidal effect of TiO_2 thin films: dynamic view of the active oxygen species responsible for the effect. J. Photochem. Photobiol. A 106, 51–56.

Kulkarni, P., Chellam, S., 2010. Disinfection by-product formation following chlorination of drinking water: artificial neural network models and changes in speciation with treatment. Sci. Total Environ. 408, 4202–4210.

Leung, T.Y., Chan, C.Y., Hu, C., Yu, J.C., Wong, P.K., 2008. Photocatalytic disinfection of marine bacteria using fluorescent light. Water Res. 42, 4827–4837.

Li, G.Y., Liu, X.L., Zhang, H.M., Wong, P.K., An, T.C., Zhao, H.J., 2013. Comparative studies of photocatalytic and photoelectrocatalytic inactivation of *E. coli* in presence of halides. Appl. Catal. B Environ. 140–141, 225–232.

Li, G.Y., Liu, X.L., An, T.C., Yang, H., Zhang, S.Q., Zhao, H.J., 2015. Photocatalytic and photoelectrocatalytic degradation of small biological compounds at TiO_2 photoanode: a case study of nucleotide bases. Catal. Today 242, 363–371.

Li, G.Y., Liu, X.L., Zhang, H.M., An, T.C., Zhang, S.Q., Carroll, A.R., Zhao, H.J., 2011. In situ photoelectrocatalytic generation of bactericide for instant inactivation and rapid decomposition of Gram-negative bacteria. J. Catal. 277, 88–94.

Luo, W., Abbas, M.E., Zhu, L.H., Deng, K.J., Tang, H.Q., 2008. Rapid quantitative determination of hydrogen peroxide by oxidation decolorization of methyl orange using a Fenton reaction system. Anal. Chim. Acta 629, 1–5.

Mukhopadhyay, S., Schellhorn, H.E., 1994. Induction of *Escherichia-coli* hydroperoxidase-I by acetate and other weak acids. J. Bacteriol. 176, 2300–2307.

Nachin, L., Nannmark, U., Nystrom, T., 2005. Differential roles of the universal stress proteins of *Escherichia coli* in oxidative stress resistance, adhesion, and motility. J. Bacteriol. 187, 6265–6272.

Nie, X., Chen, J.Y., Li, G.Y., Shi, H.X., Zhao, H.J., Wong, P.K., An, T.C., 2013. Synthesis and characterization of TiO_2 nanotube photoanode and its application in photoelectrocatalytic degradation of model environmental pharmaceuticals. J. Chem. Technol. Biotechnol. 88, 1488–1497.

Nie, X., Li, G.Y., Gao, M.H., Sun, H.W., Liu, X.L., Zhao, H.J., Wong, P.K., An, T.C., 2014. Comparative study on the photoelectrocatalytic inactivation of *Escherichia coli* K-12 and its mutant *Escherichia coli* BW25113 using TiO_2 nanotubes as a photoanode. Appl. Catal. B Environ. 147, 562–570.

Rincon, A.G., Pulgarin, C., 2007. Fe^{3+} and TiO_2 solar-light-assisted inactivation of *E-coli* at field scale – implications in solar disinfection at low temperature of large quantities of water. Catal. Today 122, 128–136.

Robertson, P.K.J., Robertson, J.M.C., Bahnemann, D.W., 2012. Removal of microorganisms and their chemical metabolites from water using semiconductor photocatalysis. J. Hazard. Mater. 211, 161–171.

Rohnstock, A., Lehmann, L., 2007. Evaluation of the probe dihydrocalcein acetoxymethylester as an indicator of reactive oxygen species formation and comparison with oxidative DNA base modification determined by modified alkaline elution technique. Toxicol. Vitro 21, 1552–1562.

Royall, J.A., Ischiropoulos, H., 1993. Evaluation of 2′,7′-dichlorofluorescin and dihydrorhodamine 123 as fluorescent-probes for intracellular H_2O_2 in cultured endothelial-cells. Arch. Biochem. Biophys. 302, 348–355.

Shi, H.X., Huang, G.C., Xia, D.H., Ng, T.W., Yip, H.Y., Li, G.Y., An, T.C., Zhao, H.J., Wong, P.K., 2015. Role of in situ resultant H_2O_2 in the visible-light-driven photocatalytic inactivation of *E. coli* using natural sphalerite: a genetic study. J. Phys. Chem. B 119, 3104–3111.

Shi, H.X., Li, G.Y., Sun, H.W., An, T.C., Zhao, H.J., Wong, P.K., 2014. Visible-light-driven photocatalytic inactivation of *E. coli* by Ag/AgX-CNTs (X = Cl, Br, I) plasmonic photocatalysts: bacterial performance and deactivation mechanism. Appl. Catal. B Environ. 158–159, 301–307.

Stone, J.R., Yang, S.P., 2006. Hydrogen peroxide: a signaling messenger. Antioxid. Redox Sign. 8, 243–270.

Storz, G., Tartaglia, L.A., Farr, S.B., Ames, B.N., 1990. Bacterial defenses against oxidative stress. Trends Genet. 6, 363–368.

Sun, H.W., Li, G.Y., Nie, X., Shi, H.X., Wong, P.K., Zhao, H.J., An, T.C., 2014. Systematic approach to in-depth understanding of photoelectrocatalytic bacterial inactivation mechanisms by tracking the decomposed building blocks. Environ. Sci. Technol. 48, 9412–9419.

Wang, H.Y.L., O'Doherty, G.A., 2012. Modulators of Na/K-ATPase: a patent review. Expert Opin. Ther. Pat. 22, 587–605.

Wang, W.J., Zhang, L.S., An, T.C., Li, G.Y., Yip, H.Y., Wong, P.K., 2011. Comparative study of visible-light-driven photocatalytic mechanisms of dye decolorization and bacterial disinfection by B–Ni-codoped TiO_2 microspheres: the role of different reactive species. Appl. Catal. B Environ. 108–109, 108–116.

Wang, W.J., Yu, Y., An, T.C., Li, G.Y., Yip, H.Y., Yu, J.C., Wong, P.K., 2012. Visible-light-driven photocatalytic inactivation of *E. coli* K-12 by bismuth vanadate nanotubes: bactericidal performance and mechanism. Environ. Sci. Technol. 46, 4599–4606.